AstroPIC II: overview of technology development for a near-infrared photonic integrated coronagraph for the Habitable Worlds Observatory

Dan Sirbu*[1], Ruslan Belikov[1], Eduardo Bendek[1,2], Kevin Fogarty[1], Rachel Morgan[1,2], Kevin Sims[1], Carson Valdez[3], Anne Kroo[3], Marek Vlk[3,4] Olav Solgaard[3], David A. B. Miller[3]

[1] NASA Ames Research Center, Moffett Field, CA
[2] SETI Institute, Mountain View, CA
[3] Ginzton Laboratory, Stanford University, Stanford, CA
[4] Department of Physics and Technology, UiT The Arctic University of Norway

ABSTRACT

This paper, the second in the series, provides an overview of continuing technology development efforts for AstroPIC, a near-infrared photonic integrated coronagraph for the Habitable Worlds Observatory (HWO). An integrated photonic coronagraph provides key advantages including reductions in size, weight, and power through miniaturization and reconfigurability through a programmable Mach-Zehnder Interferometric (MZI) mesh. We summarize the architecture of the photonic coronagraph for HWO. Key coronagraphic experimental results at Ames and Stanford testbeds include: (1) single-channel input and suppression across a single output channel measuring contrast of 6.3e-10 (92 dB) monochromatic contrast using a single diagonal of the 9-channel full upper-triangular MZI mesh first reported in the companion paper in this conference proceedings, and (2) experimental demonstration of high-efficiency grating couplers demonstrating 81-85% coupling throughput for 20 nm narrowband. A key simulation result in the companion simulation and theory paper shows that the 9-channel MZI mesh on the manufactured prototype chip enables deep contrast across a 2.5% band on a single mesh. We also provide a roadmap for the development of technology for the photonic coronagraph for HWO.

Keywords: Astrophotonics, Photonic Integrated Circuits, Exoplanets, Coronagraphy, High-Contrast Imaging, Wavefront Control, Habitable Worlds Observatory, Near-Infrared Channel

1. INTRODUCTION

The Habitable Worlds Observatory (HWO) flagship was identified as the top priority NASA flagship for astrophysics by the 2020 Decadal Survey. Planned for launch in the early 2040s, HWO will perform a direct imaging survey of approximately 100 of the nearest stellar systems and their habitable zones. The primary objective is to detect and perform spectroscopic characterization of around 25 potentially "Earth-like planets" (or "Exo-Earths"). The incorporation of an integrated photonic coronagraph can significantly enhance the scientific yields and improve technical risk margins for the telescope by improving coronagraph efficiency and miniaturizing the coronagraph instrument, enabling added functionality. The miniaturization advantages of an photonic integrated circuit (PIC) form factor addresses the volume limitations for a coronagraph instrument enabling additional channels and functionality.

PICs using components that implement a Mach-Zehnder Inteferometric (MZI) mesh are one of the key emerging technologies with potential for enhancing astronomical instrumentation ("astrophotonics"[1]) including at the recent Emerging Technologies in Astrophysics Missions (ETAM) workshop hosted by NASA.[2] AstroPIC is an integrated photonic coronagraph for HWO that provides key advantages including reductions in size, weight, and power through miniaturization and reconfigurability through a programmable Mach-Zehnder Interferometric (MZI) mesh with controllable phase shifters. Leveraging industry advancements, commercially-available PICs can be either custom-manufactured or part of multi-project wafer runs with improving turn-around times and capabilities that can benefit the design and manufacture for the integrated photonic coronagraph.

---

*email: dan.sirbu@nasa.gov

We present estimated science yields for key parametric sweeps of the integrated photonic coronagraph including end-to-end coronagraphic throughput and numbers of channels. The integrated photonic coronagraph is highly reconfigurable and adaptable. We demonstrate its compatibility with the three exploratory analytic cases (EACs) that have been considered for HWO to date. We present mission yields as parametric sweeps with respect to key pupil parameters including up to doubling of segment gaps, support struts, and the secondary obscuration diameter. In addition, the benefits of a reconfigurable photonic coronagraph that can be set to reject different stellar modes depending on the star being observed are shown through simulations showing yield sensitivities as functions of different levels of static aberrations for different coronagraph orders. We demonstrate the benefits of reconfigurability by showing optimized yields when selecting the coronagraphic order.

Further, we review the design, simulation, and recent results from our recently fabricated silicon photonic integrated circuit prototype which features multiple MZI meshes and test components that have been demonstrated across both the Ames and Stanford photonic testbeds. Key coronagraphic experimental results include: (1) single-channel input and suppression across a single output channel measuring contrast of 2.0e-9 monochromatic contrast for a 9-channel full upper-triangular MZI mesh first reported in the companion paper in this conference proceedings and (2) experimental demonstration of high-efficiency grating couplers demonstrating 81-85% coupling throughput for 20 nm narrowband. A key simulation result in the companion simulation and theory paper shows that the 9-channel MZI mesh on the manufactured prototype chip enables deep contrast across a 2.5% band on a single mesh.

These recent results highlight continued maturation of the photonic integrated coronagraph for HWO showing both the potential for deep suppression possible on-chip, improved coronagraphic throughput, and the potential for utilizing the photonic chip miniaturization advantages for broadband operation. We also provide a roadmap for the development of technology for the photonic coronagraph for HWO.

This paper has a central goal of providing an update on the AstroPIC project and the photonic coronagraph's technology development building on last year's overview,[3] summarizing key experimental and simulated developments and relevance for HWO mission. In Section 2 we review the top-level architecture of AstroPIC as a NIR coronagraph for HWO and describe at a top-level the modeling flow for obtaining science yields – these use photonic coronagraph operators implemented in the the Coronagraph Design Survey (CDS) pipeline[4] with yields obtained via the Altruistic Yield Optimizer (AYO) design reference mission simulator with the latest parameters relevant for the HWO EACs.[5] In Section 3, we summarize parametric studies using yield sensitivities for key telescope pupil parameters for the COR-12 study performed for HWO including throughput, numbers of channels, sensitivity to static aberrations, and robustness when allowing optimizing the coronagraph configuration for the current stellar observation. We also highlight additional bandwidth optimization made possible through the control of additional degrees of freedom (see simulation-focused companion paper).[6] In Section 4 we provide an overview of recent key demonstrations performed at both the Ames and Stanford photonics testbed. Details about the Ames photonics testbed and experimental results are available in the companion experimental paper.[7] These include demonstrations for a single-channel input channel optimizing suppresison in one output channel reaching 6e-10 contrast (92 dB) by configuration of the phase shifters along a single diagonal between the input and output improving on previous 7.9e-9 contrast (81 dB) demonstrated earlier as part of AstroPIC.[8] We tested first-generation AstroPIC photonic chips that featured an alternate fabrication method with improved feature size and demonstrated mesh suppression functionality across both version of the chip for normal-incidence grating couplers with 81-85% coupling – more details are available in two earlier papers.[9,10]

2. PHOTONIC INTEGRATED CORONAGRAPH

Any optical system (with conventional components such as mirrors, lenses, masks, etc.) that has an input plane and an output plane is mathematically equivalent to a linear passive operator transforming the electric field at the input plane into another electric field in the output plane and can be represented by a linear operator.[11,12] An optimal linear operator for the coronagraph can be computed (which removes specific low order modes from input to the output plane) with corresponding science yields several times greater than for traditional coronagraphs, and these are largely independent of aperture obstructions, segmentations, or struts and can significantly relax sensitivities to aberrations.

The significance of a photonic coronagraph for HWO is driven by the paradigm-shift enabled by PICs, in particular a forward mesh of Mach-Zehnder Interferometers ("MZIs") with tracked phase delays can implement a universal linear operation[13] and thus implement the functionality of any conceivable optical system (including an optimal coronagraph in the limit of a large number of modes).
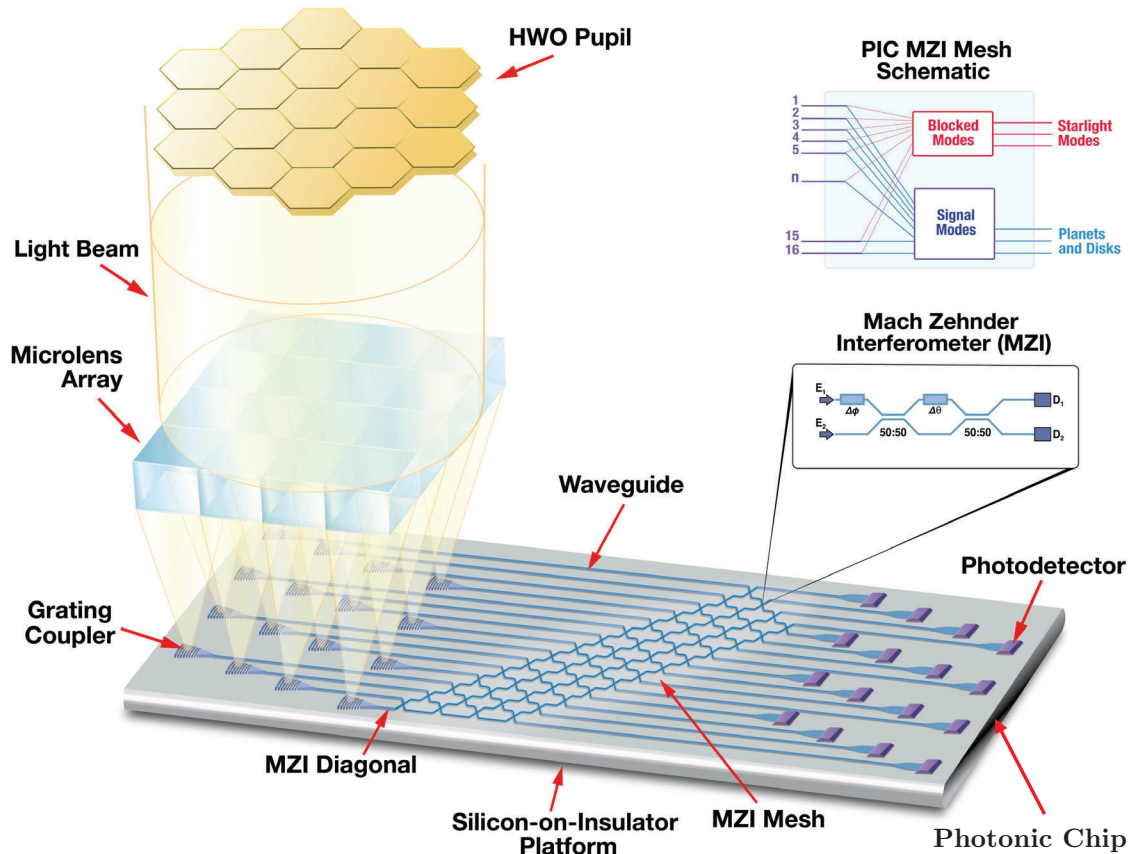

Figure 1: Illustration of AstroPIC photonic integrated coronagraph for HWO shown here with 16 input channels – the architecture can be scaled up with additional channels. A free-space optical beam from the telescope pupil is coupled using a microlens array onto a PIC device. At the focus of each individual lenslet is a grating coupler that feeds that portion of the input beam onto an individual waveguide, and represents a single input channel. Each input channel represents a mode or basis vector in an orthogonal basis (16-dimensional, in this example), and the coupling operation projects the input beam onto that basis. Each input mode/waveguide contains a mix of noise (starlight) and signal (planet and disk light). The MZI mesh (here shown with 4 diagonals) transforms the input basis into an output basis where the starlight is maximally concentrated in as few output modes as possible. The remaining output modes contain mostly light from planets and disks. The intensities of output modes are captured by on-chip photodetectors (as shown) or coupled out to an external detector and can be configured to contain maximal light from each individual planet (or represent samples on an image or Lyot plane). The actual mesh uses equal path lengths to maintain coherence at each MZI.

Thus, PICs provide a practical means to implement near-optimal coronagraphy providing key advantages via a compact footprint. This has the potential to improve both science and cost margins while reducing risk. By improving the efficiency and effectiveness of the overall observatory, a photonic coronagraph instrument increases the yield of exoplanet discoveries, enables more relaxed aperture requirements, accommodating wider struts, larger segment gaps, larger secondary obstructions, and less stringent stability requirements. The photonic coronagraphic mesh can also be dynamically reconfigured for individual observations to select an appropriate
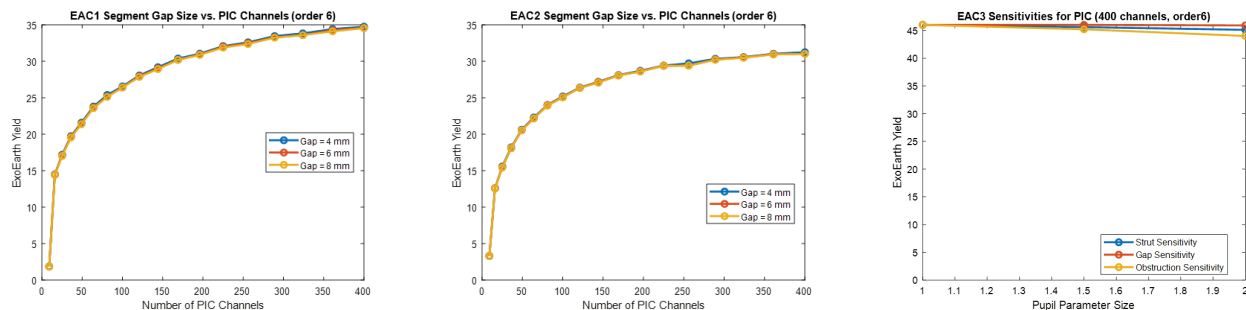
Figure 2: Integrated photonic coronagraph robustness of characterized exo-Earth yield as function of number of spatial channels and pupil-feature oversizing (1–2×) for three HWO EACs evaluated in COR-12. (Left) EAC-1: off-axis, hexagonally segmented; segment-gap scale varied. (Center) EAC-2: off-axis, keystone segmentation; segment-gap scale varied. (Right) EAC-3: on-axis, hexagonal segmentation with secondary obscuration and support struts; all features scaled.

trade-off between tolerance to low order modes and inner working angle (IWA).

The AstroPIC photonic integrated coronagraph for HWO is shown in Fig. 1 with a 16-mode spatial representation (that can be scaled-up to additional modes). It comprises (1) a lenslet array that samples the telescope pupil and focuses light into an array of grating couplers, (2) grating couplers that inject an orthogonal set of PIC input modes, (3) an MZI mesh that transforms the input modes into an output basis to optimally separate signal (planet/disk) from starlight, and (4) on-chip photodetectors (or, alternatively, off-chip detectors fed by edge-coupled fibers). By programming the mesh, the detector array can realize an image plane, a Lyot plane, or any other convenient plane. If planet locations are known, individual output modes can be tuned to maximize throughput from each target.

We configure the MZI mesh by tuning the two phase shifters in each interferometer (see Fig. 1). Actuation can be thermo-optic heaters (our current baseline), MEMS, or electro-optic devices. We assume ideal components, such as perfect phase shifters, lossless couplers, and no back-reflections. Each MZI implements a tunable beam splitter (a 2-input 2-output rotation of the input fields). Phase settings are computed with an inverse-propagation algorithm.[13] The coronagraph's contrast, IWA, and throughput are determined by the number of starlight modes "blocked," which defines the coronagraph order. These modes can also be used for a low-order wavefront sensor (LOWFS).

3. RELEVANCE TO HWO

We have developed a simulation pipeline[6] used to predict the science yield of different configurations of the AstroPIC coronagraph for HWO, enable photonic coronagraph architecture trades, and identify areas of greatest impact for additional technology development and maturation. In addition, this simulation pipeline can be used to validate predicted performance against experimental results and to optimize the coronagraphic mesh configuration for improved performance including bandwidth and for wavefront control of aberrations.

The simulation pipeline consists of several key modules. First, a free-space coupling module that enables representation of the propagation of electric field from the telescope pupil (including potentially any upstream optics of the coronagraph), through the microlens array to complex-valued electric field amplitudes that sample the full-telescope pupil at the grating couplers and represent the input to the MZI mesh. Second, the MZI mesh itself is implemented in a matrix that represents a mapping between output channels, diagonals across the mesh and input channels performing the energy sorting to the output electric field vector. Idealized propagation through a full upper triangular Reck mesh[14] enables decomposition of any unitary matrix through the MZI mesh (with the Reck layout using symmetrical, balanced paths through additional path length structured added for phase matching along each path). The layout and energy sorting functionality is compatible with a more compact Clements mesh[15] or a series of binary-trees.
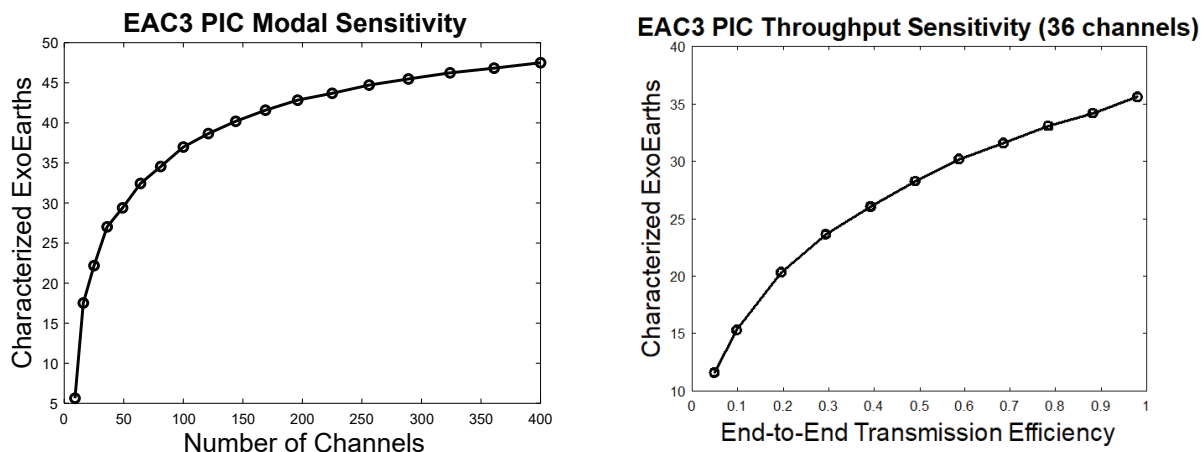
Figure 3: Yield sensitivity of the photonic coronagraph to key parameters for HWO EAC-3. Left: number of characterized exo-Earths vs. pupil-sampling spatial modes. Right: number of characterized exo-Earths vs. end-to-end transmission efficiency.

On the back-end of the mesh, we implement a conversion to an equivalent Lyot plane. This serves as the output plane and provides an interface for the photonic integrated coronagraph operator to the Coronagraph Design Survey (CDS).[4] This interface and near-optimal performance of the PIC-operator limited by the number of modes was described in the previous paper in the AstroPIC technology development series.[3] Using the CDS framework, it is possible to create yield input packages to provide input to design reference mission (DRM) simulators such as the AYO[16] and ExoSIMS.[17] The yield results obtained here have been been currently evaluated with AYO via the FRIDAY server, with an ExoSIMS evaluation currently in progress.

We assume a 20% bandwidth, consistent with current coronagraphs. The photonic coronagraph's small mass and volume enable multi-band layouts: split the spectrum with either an external dichroic (or on-chip wavelength splitting components) and route each band to dedicated grating couplers and (i) MZI meshes on the same wafer, (ii) stack multiple PICs tuned to different bands, or a combination of both. Thus 20% is not a physical limit; stacked or parallel meshes can extend bandwidth and enable simultaneous multi-channel characterization. In companion simulations, a single MZI mesh achieved $\sim 10^{-10}$ contrast over 2.5% bandwidth by optimizing additional degrees of freedom beyond the monochromatic case. Tiling a 20% band with ~ 8 such 2.5% sub-bands would therefore require only a practical number of meshes and MZI meshes, keeping device scale feasible. Furthermore, additional optimization could extend the bandwidth on a single mesh beyond 2.5%.

This interface allows performing parametric sweeps of different telescope apertures, aberrations, and photonic coronagraph operators to determine yield sensitivities. In each case, a new photonic coronagraph is configured to account for the updated telescope pupil and corresponding yield simulations performed. In the parametric study HWO COR12, we evaluated the robustness of PIC-based coronagraphs by measuring the characterized exo-Earth yield under 1–2× pupil-feature oversizing across three entrance-aperture candidates (EACs) as shown in Figure 2. For EAC-3 (on-axis, hexagonally segmented with a secondary and struts), we swept strut widths of 80, 120, and 160 mm; segment gaps of 6, 9, and 12 mm; and central-obscuration diameters of 800, 1200, and 1600 mm. For EAC-1 and EAC-2 (off-axis hexagonal/keystone), we varied segment gaps of 4, 6, and 8 mm. Across all cases, PIC designs were nearly insensitive to feature-size changes; the small yield impacts observed are driven primarily by increased obscuration fraction from the oversized pupil features.

Using our mesh simulation pipeline, we can probe yield sensitivities via parameter sweeps of the photonic coronagraph itself. For EAC-3 operators with typical assumptions for EAC-3 incorporated into FRIDAY scenarios, Fig. 3 shows (left) characterized exo-Earths vs. the number of PIC spatial channels sampling the pupil and (right) characterized exo-Earths vs. end-to-end throughput. While absolute yields depend on mission assumptions, the trends are robust: $\sim$25 channels meet the HWO baseline goal (25 exo-Earths) and $\sim$100 channels recover $\sim$80% of the asymptotic yield. Similarly, for throughput sweeps: $\geqslant$40% end-to-end transmission is required to reach the baseline goal, and $\gtrsim$30% already recovers substantial science performance.
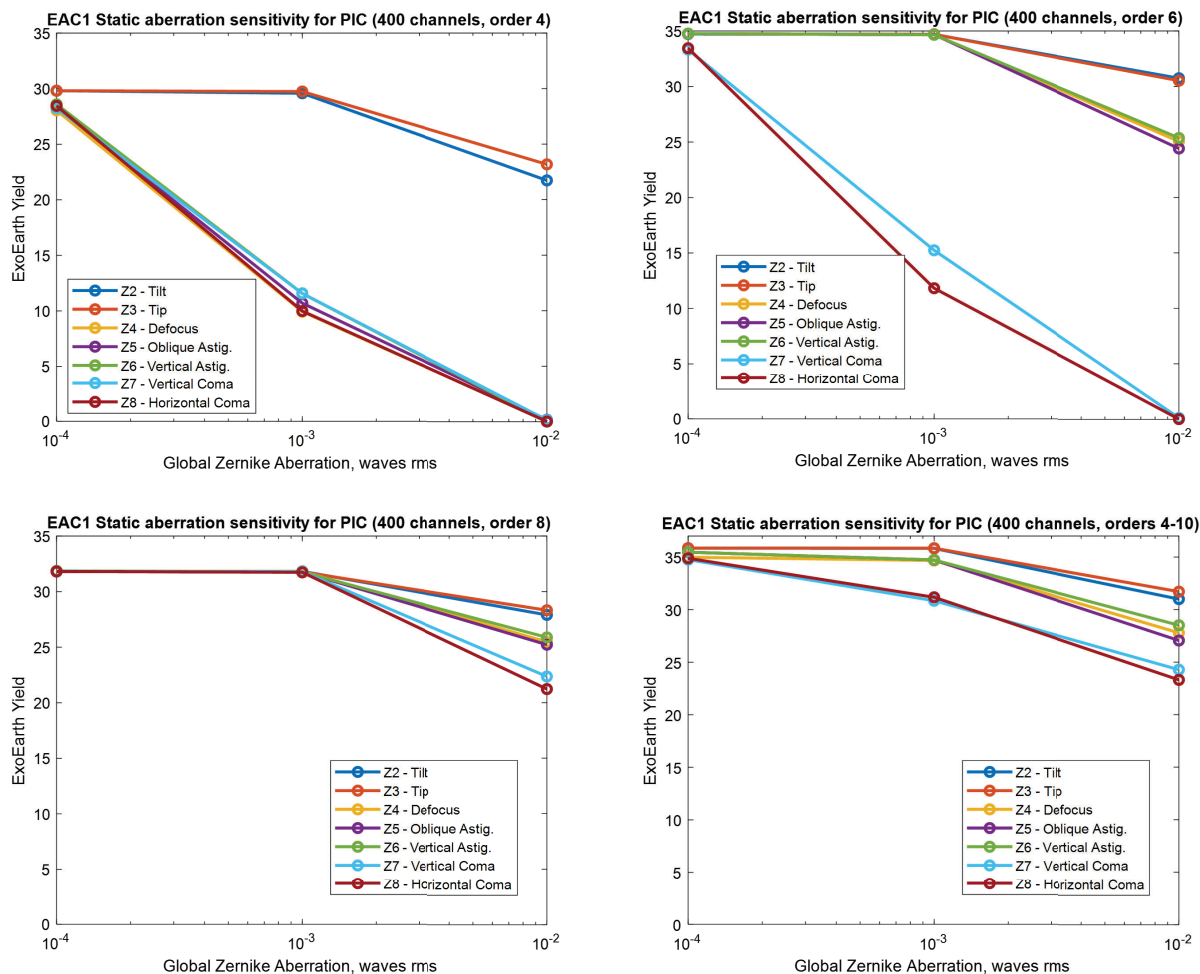
Figure 4: Yield sensitivity of a photonic coronagraph to global Zernike aberrations Z_2-Z_8 applied to the EAC-1 pupil over 10^{-4} to $1-2$ waves rms. Top-left: order-4 is robust to Z_2-Z_3 (tip/tilt). Top-right: order-6 is robust to Z_2-Z_6 (adds defocus, astigmatism). Bottom-left: order-8 adds robustness to Z_7-Z_8 (coma, trefoil) with some yield cost. Bottom-right: per-target order optimization maximizes characterized exo-Earth yield and improves robustness to static aberrations.

For EAC-1 with a 400-channel photonic coronagraph, we sweep global Zernike amplitudes Z_2-Z_8 from 10^{-4} to $1-2$ waves rms to explore exoearth candidate yield behavior in the presence of static aberrations applied at the telescope pupil as shown in Figure 4. With a 4th-order setting the coronagraph blocks tip and tilt while passing higher orders; moving to a 6th-order setting also rejects defocus and astigmatism; an 8th-order setting further blocks coma and trefoil at some cost in characterized yield. Selecting the coronagraph order per target makes effective use of the PIC's reconfigurability and maximizes yield in the presence of these static aberrations. Although only static aberrations are evaluated here, the same reconfigurable strategy can be applied in the future to dynamic aberrations and can be combined with wavefront control to further improve performance.

Two practical paths emerge[3]. A hybrid approach uses a modest PIC (about 16–36 spatial modes) as a pick-off inside the traditional coronagraph's IWA, providing additional science signal and optionally serving as a LOWFS sensor with near-term manufacturability. A full-photonic chip with hundreds of channels (e.g., 400) operates as a stand-alone coronagraph whose reconfigurable modes offer the greatest science return, but it requires further maturation in contrast, throughput, bandwidth, and robustness before flight. Alternatively, the full-photonic coronagraph instrument can be deployed during servicing which HWO will be built to support.
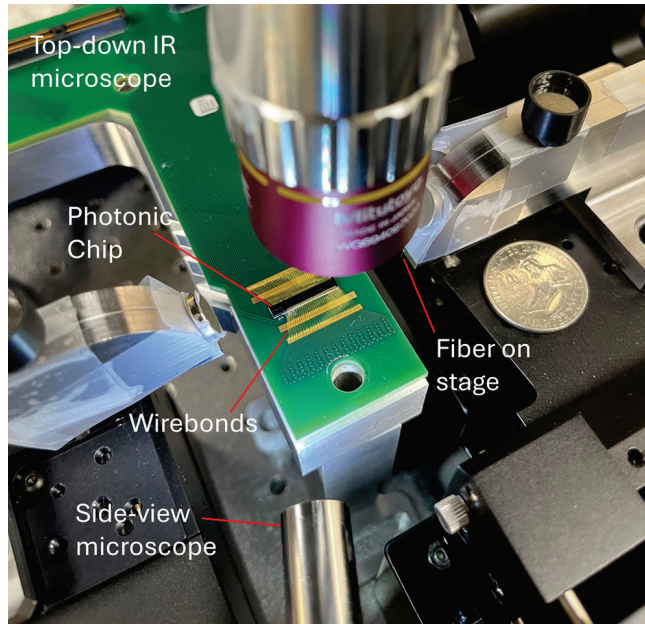
Figure 5: Photonic test station at the Ames Coronagraph Testbed showing the top-down IR and side-view optical microscope for alignment, the input and output fibers on alignment stages, the photonic chip wirebonded to the printed circuit board.

4. EXPERIMENTS

In this section, we summarize recent experimental progress demonstrating key coronagraph functionality across both the existing Stanford photonics testbed and the newly commissioned photonics testbed at NASA Ames. These experiments validate the photonics testbed at Ames, demonstrate deeper photonic nulling levels on-chip using a single-input and output channel than in previous experiments, and validate the recently manufactured commercial chips that have been manufactured and wire-bonded.

4.1 Photonics testbeds

The AstroPIC photonics test station at the Ames Coronagraph Testbed is shown in Figure 5. The testbed status and recent experimental results are described in detail in the companion paper,[7] and is geared to system-level demonstrations and deep-contrast performance with realistic HWO-like pupils. The photonics teststation itself is modeled on the testbed at Stanford, which is focused on component-level development and testing. The Ames testbed targets 1×10^{-9} contrast for a single input channel and other on-chip demonstrations and 1×10^{-7} contrast with an HWO-like pupil. The setup supports free-space and fiber coupling on/off chip, programmable phase shifters across the MZI mesh, and readout from on-chip photodetectors enabling measurement of 1×10^{-10} contrast. Other features include PIC thermal control and top-view IR plus side-view visible microscopy for alignment and diagnostics. The Stanford testbed emphasizes novel functionality and component validation (e.g., inverse-designed high-efficiency grating couplers), while the Ames testbed focuses on deep contrast measurements, end-to-end performance validation and compatibility with HWO. The Ames testbed has been recently commissioned achieving first-light demonstrating: (1) injection of a single fiber into an uncontrolled MZI mesh, (2) measurement of output light from the uncontrolled mesh, and (3) active switching by the control of phase shifters for an MZI element.

4.2 Manufactured chips

Earlier this year we received the first AstroPIC chips that have fabricatted at two foundries.[3] The Cycle-1 AstroPIC chip has been taped out and fabricated at two different commercial foundries that utilize different manufacturing methods. Advanced Microfoundries (AMF) uses standard photolithography for multi-project wafer (MPW) leveraging the same foundry flow as the initial experiment demonstrated for AstroPIC that used
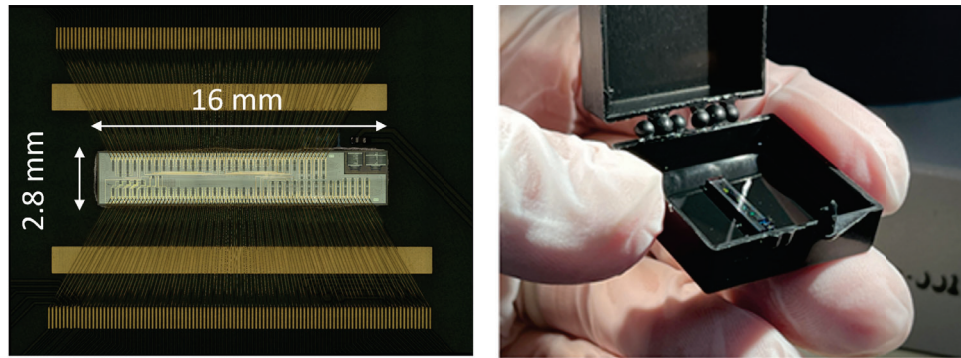
Figure 6: Manufactured AstroPIC photonic chip with two independent coronagraphic MZI meshes and on-chip test structures. (Left) Microscope image after wirebonding chip to host circuit board with chip dimensions indicated (courtesy of Silitronics Inc.). (Right) Handheld photonic integrated coronagraph chip illustrating instrument miniaturization.

an existing MZI mesh.[8] This existing prototype[18] had achieved 7.9e-9 (81 dB) contrast in a single input channel minimizing output suppression. After fabrication, a printed circuit board for the electrical interface to the chip was also commercially manufactured. The photonic chip has been commercially wirebonded by Silitronics Inc. as shown in the left-hand side of Figure 6. For scale, a handheld photonic integrated coronograph display unit is shown illustrating the miniaturization potential for astrophotonic-based instrumentation. A similar layout was submitted to Applied Nanotools (ANT) which uses e-beam lithography – this process features improved feature sizes and smaller-batch custom runs providing process flexibility for an additional etch step and allowing the addition of a set of test structures to fabricate high-efficiency "three-wave" grating couplers that were optimized via inverse design.[9] Additional packaging with bonded fiber array units for output coupling is in progress.

The photonic coronagraph device consists of a silicon-on-insulator PIC ($2.8 \, \text{mm} \times 16 \, \text{mm}$ reticle) with $1.55 \, \mu\text{m}$ directional couplers and input/output grating couplers, and integrates two coronagraphic meshes plus exploratory test structures. The first mesh is a triangular MZI mesh with 9 input modes and 9 diagonals; a 3×3 input grating array supports free-space coupling via a microlens array, with bond-pad count setting phase-shifter and mode limits. This device enables higher-mode free-space experiments and measurements of throughput, inner/outer working angles, and deep contrast, with grating couplers expected to be the main limitation on throughput. The second mesh is a 7-input, 4-diagonal Perfect-MZI (PMZI) mesh that doubles phase shifters per cell to reduce cross-channel leakage and target $\sim 10^{-9}$ contrast, trading increased device complexity for deeper nulls. Additional structures sweep directional-coupler parameters for broadband tuning and include custom input couplers for band and polarization separation (e.g., dual-polarization tests).

4.3 Photonic nulling at 6.3e-10 contrast (92 dB), single-channel, monochromatic

To date, in-air demonstrations of AstroPIC prototypes have achieved very promising results. The first suppression experiment at the Ames Photonics Testbed used the 9-input full upper triangular MZI mesh described above for the AMF chip and utilized a single-diagonal with 8-MZI elements and is the key result described in the companion experimental paper.[7] In this experiment, input light is coupled using a single-mode fiber into a single grating coupler and a fiber is coupled to an output grating coupler that uses the longest diagonal of the 9-mode triangular mesh. The MZIs along the top diagonal are configured to minimize the power measured from the output port. The input laser is monochromatic and set to 1.55 µm. The total power across all output modes is measured at the beginning and end of each experiment, and is used to compute the total contrast. The contrast measured at the end of this configuration process measured 2.0e-9 contrast (87 dB) with measured throughput end-to-end on the chip of 9.5%. Repeating this procedure with a chip fabricated by ANT yielded an even better 6.3e-10 contrast (92 dB), but with slightly worse end-to-end measured throughput on-chip of 8.7%. The suppression improvement on the e-beam lithography chip may not be due to the manufacturing method, but rather higher resolution of voltage input resolution using the same interface board. The end-to-end measured throughput, for both chips, of approximately 10% is to the previous prototype used,[3] and continued to be dominated by losses

from standard, foundry-provided input and output grating coupler with approximately 30% coupling efficiency; silicon waveguide propagation losses at 1.55 um are ∼1 dB/cm.

This suppression experiment is the first performed at the recently commissioned Ames Photonics Testbed and demonstrated a factor of 10× improvement over the previous best suppression measured.[8] The significance of this result it demonstrates a deeper contrast level measured on-chip than previously which is made possible by the additional MZI stages in the larger 9-channel mesh. In addition, it also validates the measurement sensitivity of the testbed to levels approaching 1e-10 contrast in-air. Continued improvements on the recently commissioned testbed to improve stability, operational improvements obtained from measuring multiple output channels simultaneously once the FAU-bonded unit becomes available, as well as the free-space coupling module to couple a telescope pupil relevant for HWO will provide additional capability and potential for deeper contrast demonstrations. In addition, these tests demonstrate that meshes fabricated with both foundries are fully functional and can achieve similar performance.

4.4 Three wave interaction grating (TWIG) couplers with 81-85% coupling efficiency

One of the key performance drivers for the photonic integrated coronagraph is maximizing end-to-end coupling throughput. From previous experiments for the photonic coronagraph, the standard foundry gratings[19] utilized to couple light on and off-the chip have been shown to dominate throughput losses[3,10] and this also applies to the latest generation of photonic chips.[7] These foundry gratings are designed for a ∼ 10° angle of incidence at 1550 nm (with the optimal coupling angle depending on wavelength), which is inconvenient from an instrument design perspective. As a result, part of this AstroPIC technology development program has focused on designing novel normal-incidence free-space grating couplers with high efficiency for future iterations of AstroPIC prototypes.

Traditionally, normal-incidence grating couplers are challenging to design in silicon photonics due to the material symmetry limiting the total possible efficiency to 50%. This can be resolved by adding additional etch steps to have more complicated features, but this becomes difficult to achieve using the practical limitations on minimum-feature sizes offered using photolithography in fabrication. The new AstroPIC grating couplers take advantage of smaller feature sizes by transitioning to a foundry that offers electron beam (e-beam) lithography, which is capable of fabricating much smaller features with more flexible layer heights at the expense of reduced scalability. The new designs utilize the destructive interference of the downward and backward-scattering waves from each grating feature (and hence are named "three wave interaction grating," or TWIG) to minimize dominant sources of coupling loss from back-scatter and substrate scatter, and are designed using adjoint optimization. 2D finite-difference time domain (FDTD) simulations showed that optimizing for coupling efficiency and trading bandwidths could enable grating couplers with three different designs reaching 98.6%, 95.6%, and 93.4% peak coupling efficiency and corresponding 1 dB bandwidths of 8 nm, 29 nm, and 58 nm centered around 1.55 um (C-Band).[9] A grating design that had 91% coupling efficiency and a 34 nm bandwidth in 3D FDTD simulation was selected for the first fabrication run.

To account for uncertainty in fabrication error, several variations of this design were generated by sweeping over expected sources of error such as layer misalignment and etch width or depth error. Each variant was fabricated in both a 1D configuration where a long adiabatic taper expands the mode from a single mode waveguide width to the grating width followed by straight grating teeth and a focusing configuration where a shorter non-adiabatic taper is used to expand the mode and the grating teeth are curved to account for the resulting bending in the wavefront. Of the designs fabricated, the highest performing designs achieved a 81% coupling efficiency in the 1D configuration and 85% coupling efficiency in the focusing configuration over a 20 nm bandwidth. These TWIG couplers were designed and tested in the Stanford University's Solgaard Lab within the Electrical & Computer Engineering (ECE) Department. These demonstrated excellent agreement between the expected simulation of the manufactured grating couplers and the measured throughput performance. A summary of the performance versus simulation results is summarized in Table 1. The fabrication tolerances reported by the foundry included etch-width bias of ± 10 nm, which shifted the central spectrum with over-etching causing a combined blue shift and broadening, and alignment errors of ± 10 nm having minor impacts on efficiency and bands. These errors were compensated by a parametric sweep and testing structures to identify the best match.

Table 1: TWIG vertical grating couplers: experiment vs. simulation (SOI, C-band).

Device	Experiment			Simulation (optimized)	
	Peak Eff. (%)	Peak λ (nm)	1 dB BW (nm)	Peak Eff. (%)	1 dB BW (nm)
1D TWIG	81.1	1555.5	20	91	34
Focusing TWIG	85.4	1546.4	20	91	34

Notes: Experimental values are for the best devices measured. Simulated values correspond to the optimized TWIG design used as the basis for both 1D and Focusing variants; the simulated 1 dB bandwidth spans C-band (about 1530–1564 nm).

Table 2: Summary of AstroPIC experimental suppression results to date

Experiment	Architecture / Config	Extinction (linear / dB)	Actively controlled MZI elems.
Single-channel nulling	4-MZI mesh (dual-config min/max)	1×10^{-7} / 70 dB	4
Single-channel nulling	3-input triangular mesh with PMZIs along main path	7.9×10^{-9} / 81 dB	6
Single-channel nulling	9-input triangular mesh (photolithography); single diagonal path controlled	2.0×10^{-9} / 87 dB	8
Single-channel nulling (deepest to date)	9-input triangular mesh (e-beam lithography); single diagonal path controlled	6.3×10^{-10} / 92 dB	8
Free-space demo	4-channel PIC; on-axis suppression and off-axis throughput	1×10^{-4} / 40 dB	3

5. TECHNOLOGY DEVELOPMENT ROADMAP

State of the art demonstrations of PICs in the lab have advanced rapidly and significantly over the past several years, to levels that are becoming relevant and enticing to HWO, however at this point these are primarily best classified as "component-level" demonstrations. These include demonstrations of high-efficiency coupling of light into a chip (without coronagraphic functionality[10,20]), rapidly improving starlight suppression with a small number of channels that has now reached 6e-10 contrast (without demonstrating a high-efficiency coupling into the chip[7,8]) as well as industry-led development that demonstrate spatial sampling of beams with tens of thousands of input channels (but without demonstrating coronagraphic functionality). In Table 2 we summarize experimental demonstrations focused on enabling deep suppression to reach deep suppression ratios on-chip with different architectures/configurations as part of the AstroPIC project to date, and a free-space coupling demonstration. The next steps for the AstroPIC project and the recently commissioned testbed at NASA Ames will be to perform a system-level free-space coupling demonstration to reach TRL 3.

Figure 7 presents a proposed PIC roadmap to TRL-5, summarizing the current state of the art, the path to TRL-3 before the start of this work, the expected advances from future work, and subsequent advancement to TRL-5 for enabling injection of a photonic coronagraph onto HWO. The proposed development path will raise the technology readiness of the photonic integrated coronagraph system in NIR for a pupil relevant to HWO to TRL-4, enabling consideration of a NIR-based channel as part of HWO trade studies featuring small mass and volume constraints and an aggressive IWA for exoplanet characterization prior to the start of Phase A which will include demonstrations in relevant environments and additional cycles of component optimization and integration into future tape-outs of the AstroPIC photonic coronagraph.

6. CONCLUSIONS

In this paper, we have provided an overview on the continuing progress on technology development for the AstroPIC photonic coroangraph. In addition to the miniaturization potential of an astrophotonic coronagraph
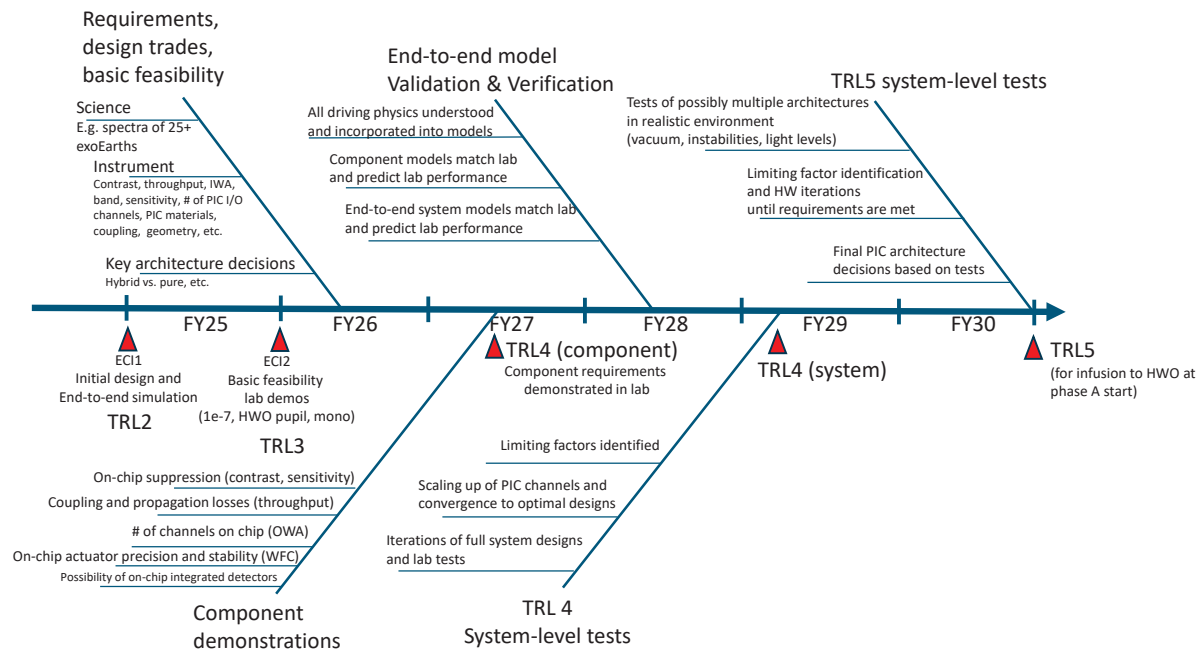
Figure 7: Technology development roadmap for the photonic integrated coroangraph shows progress achieved by the end of the AstroPIC project to TRL-3, proposed TRL-4 component and system milestones and path to a photonic instrument integration into HWO prior to project Phase A.

instrument, we have shown through the optimization and modeling pipeline the potential benefits in terms of science yields and flexible reconfiguration of the PIC for the HWO mission architecture. We have shown that a PIC-based photonic coronagraph is widely compatible with all EACs considered to date by the HWO project, and have shown that the photonic coronagraph is robust to significant variations in all telescope pupil parameters. In addition, we have shown the benefits in reconfigurability in terms of tailoring the photonic coronagraph to specific target observations and static aberrations, showing significant improvements in robustness and yield in the presence of varying levels of aberrations. We have shown that improvements that are now within reach in both coronagraphic throughput and a modest number of channels can enable a hybrid coronagraph to operate at first light, and a scaled fully photonic coronagraph with hundreds of modes can be added to HWO during servicing to augment its coronagraphic capabilities and efficiency. Furthermore, a key simulation result shows that additional degrees of freedom on an MZI mesh can be utilized to improve coronagraphic functionality – for example, supporting a 1e-10 contrast in a 2.5% band on a single MZI mesh,[6] which enables the realization of broadband photonic coronagraphs with relatively small numbers of parallel meshes.

The photonic testbed at the Ames Coronagraph Testbed has now been commissioned. The recently manu-factured and packaged AstroPIC photonic coronagraph has demonstrated 6.3e-10 contrast (92 dB) on the chip representing an improvement of a factor of 4x compared to previous results.[7] Finally, a component optimization effort has designed, fabricated, and experimentally verified normal-incidence high-efficiency grating couplers with measured coupling efficiencies ranging from 81% - 85% and demonstrating excellent agreement with the expected design simulation.

Future steps include demonstrations with a free-space coupling module with a representative HWO pupil coupled to demonstrate coronagraphic suppression in the presence of additional input channels. Further, a photonic source that simulates both the star and the planet is planned.[21]

ACKNOWLEDGMENTS

REFERENCES

[1] N. Jovanovic *et al.*, "2023 Astrophotonics Roadmap: pathways to realizing multi-functional integrated astrophotonic instruments," *J. Phys. Photonics* **5**, 2021.

[2] NASA Astrophysics Division, "Emerging technologies in astrophysics missions." `https://www.nasa.gov/emerging-technologies-for-astrophysics-missions-workshop/`, 2025. (accessed 21 August 2025).

[3] D. Sirbu, R. Belikov, K. Fogarty, C. Valdez, Z. Sun, A. Kroo, O. Solgaard, D. A. B. Miller, and O. Guyon, "Astropic: near-infrared photonic integrated circuit coronagraph architecture for the habitable worlds observatory," in *Space Telescopes and Instrumentation 2024: Optical, Infrared, and Millimeter Wave*, L. E. Coyle, S. Matsuura, and M. D. Perrin, eds., *Proc. SPIE* **13092**, p. 130921T.

[4] R. Belikov *et al.*, "Coronagraph design survey for future exoplanet direct imaging space missions," *Proc. SPIE* **13092**, 2024.

[5] C. Stark *et al.*, "The ExoEarth Yield Landscape for Future Direct Imaging Space Telescopes," *JATIS* **5**(2), 2019.

[6] K. Fogarty, D. Sirbu, R. Morgan, E. Bendek, and R. Belikov, "Modelling and optimization pipeline for the astropic coronagraph," in *Space Telescopes and Instrumentation 2025: Optical, Infrared, and Millimeter Wave*, *Proc. SPIE* **13627**, p. 1362782.

[7] R. Morgan, E. Bendek, K. Fogarty, A. Kroo, C. Valdez, M. Vlk, O. Solgaard, D. A. B. Miller, and D. Sirbu, "Testbed design and high-contrast demonstration with the AstroPIC integrated photonic coronagraph," in *Space Telescopes and Instrumentation 2025: Optical, Infrared, and Millimeter Wave*, *Proc. SPIE* **13627**, p. 1362726.

[8] C. G. Valdez, Z. Sun, A. R. Kroo, D. A. B. Miller, and O. Solgaard, "High-contrast nulling in photonic meshes through architectural redundancy," *Opt. Lett.* **50**(11), pp. 3660–3663, 2025.

[9] C. G. Valdez, S. Pai, P. Broaddus, and O. Solgaard, "High-efficiency vertically emitting coupler facilitated by three wave interaction gratings," *Opt. Lett.* **49**(9), pp. 2373–2376, 2024.

[10] C. G. Valdez, S. A. Bongarz, A. R. Kroo, A. J. Miller, M. J. F. Digonnet, D. A. B. Miller, and O. Solgaard, "Three-wave interaction grating coupler with sub-decibel insertion loss at normal incidence." arXiv:2506.19242 [physics.optics], 2025. v1, submitted 24 Jun 2025.

[11] O. Guyon, E. Pluzhnik, M. Kuchner, B. Collins, and S. Ridgway, "Theoretical limits on extrasolar terrestrial planet detection with coronagraphs," *ApJS* **167**, 2006.

[12] R. Belikov, D. Sirbu, J. Jewell, O. Guyon, and C. Stark, "Theoretical performance limits for coronagraphs on obstructed and unobstructed apertures: How much can current designs be improved?," *Proc. SPIE* **11823**, 2021.

[13] D.A.B. Miller, "Self-configuring universal linear optical component," *Phot. Res.* **1**, 2013.

[14] M. Reck, A. Zeilinger, H. J. Bernstein, and P. Bertani, "Experimental realization of any discrete unitary operator," *Physical Review Letters* **73**(1), pp. 58–61, 1994.

[15] W. R. Clements, P. C. Humphreys, B. J. Metcalf, W. S. Kolthammer, and I. A. Walmsley, "Optimal design for universal multiport interferometers," *Optica* **3**(12), pp. 1460–1465, 2016.

[16] C. C. Stark, B. Mennesson, S. T. Bryson, E. B. Ford, T. D. Robinson, R. Belikov, M. R. Bolcar, L. D. Feinberg, O. Guyon, N. Latouf, A. M. Mandell, B. J. Rauscher, D. Sirbu, and N. W. Tuchow, "Paths to robust exoplanet science yield margin for the Habitable Worlds Observatory," *Journal of Astronomical Telescopes, Instruments, and Systems* **10**(3), p. 034006, 2024.

[17] D. Savransky, R. Knight, M. Turmon, C. Spohn, R. Morgan, M. Damiano, G. Genszler, and J. Kulik, "Quantifying the impacts of schedulability on science yield of exoplanet imaging missions," in *Techniques and Instrumentation for Detection of Exoplanets XI*, G. J. Ruane, ed., **12680**, p. 126801K, International Society for Optics and Photonics, SPIE, 2023.

[18] S. Pai, Z. Sun, *et al.*, "Experimentally realized in situ backpropagation for deep learning in photonic neural networks," *Science* **380**, 2023.

[19] R. Marchetti, C. Lacava, A. Khokhar, X. Chen, I. Cristiani, D. Richardson, G. Reed, P. Petropoulos, and P. Minzioni, "High-efficiency grating-couplers: demonstration of a new design strategy," *Scientific reports* **7**(1), p. 16670, 2017.

[20] D. McKeithen, J. Jewell, and J. K. Wallace, "Hardware development towards the demonstration of an ideal photonic coronagraph," in *Space Telescopes and Instrumentation 2024: Optical, Infrared, and Millimeter Wave*, L. E. Coyle, S. Matsuura, and M. D. Perrin, eds., **13092**, p. 130925V, International Society for Optics and Photonics, SPIE, 2024.

[21] E. Bendek, M. Noyes, B.-J. Seo, G. Ruane, H. Nejadriahi, R. Belikov, and D. Sirbu, "Photonic source for binary source simulations," in *245th American Astronomical Society Meeting*, 2025.